IEEE Access
Multidisciplinary ⋮ Rapid Review ⋮ Open Access Journal

Received 7 December 2022, accepted 19 December 2022, date of publication 21 December 2022,
date of current version 28 December 2022.

Digital Object Identifier 10.1109/ACCESS.2022.3231330

RESEARCH ARTICLE

Enhanced RGB-Based Basis Pursuit Sparsity Averaging Using Variable Density Sampling for Compressive Sensing of Eye Images

GANDEVA BAYU SATRYA[1], (Senior Member, IEEE), I. NYOMAN APRAZ RAMATRYANA[2], (Member, IEEE), LEDYA NOVAMIZANTI[3], (Member, IEEE), AND SOO YOUNG SHIN[2], (Senior Member, IEEE)

[1]School of Applied Science, Telkom University, Bandung 40257, Indonesia
[2]Department of IT Convergence Engineering, Kumoh National Institute of Technology, Gumi 39177, South Korea
[3]School of Electrical Engineering and Humic Engineering, Telkom University, Bandung 40257, Indonesia

Corresponding author: Gandeva Bayu Satrya (gandevabs@ieee.org)

This work was supported in part by the Directorate of Research and Community Service, Telkom University; in part by the Ministry of Science and ICT (MSIT), South Korea, under the Grand Information Technology Research Center Support Program supervised by the Institute for Information communications Technology Planning Evaluation (IITP), under Grant IITP-2022-2020-0-01612; and in part by the Priority Research Centers Program through the National Research Foundation of Korea (NRF) funded by the Ministry of Education, Science and Technology, under Grant 2018R1A6A1A03024003.

ABSTRACT Compressive sensing (CS) plays a critical role in sampling, transmitting, and storing the color medical image, i.e., magnetic resonance imaging, colonoscopy, wireless capsule endoscopy, and eye images. Although CS for medical images has been extensively investigated, a challenge remains in the reconstruction time of the CS. This paper considers a reconstruction of CS using sparsity averaging (SA)-based basis pursuit (BP) for RGB color space of eye image, referred to as RGB-BPSA. Next, an enhanced RGB-BPSA (E-RGB-BPSA) is proposed to reduce the reconstruction time of RGB-BPSA using a simple SA generated by the combination of Daubechies-1 and Daubechies-8 wavelet filters. In addition, variable density sampling is proposed for the measurement of E-RGB-BPSA. The performance metrics are investigated in terms of structural similarity (SSIM) index, signal-to-noise ratio (SNR), and CPU time. The simulation results show the superior E-RGB-BPSA over the existing RGB-BPSA at an image with a resolution 512×512 pixels into a measurement rate 10% with SSIM of 0.9, SNR of 20 dB, and CPU time of 20 seconds. The E-RGB-BPSA can be a solution to massive data transmissions and storage for the future of medical imaging.

INDEX TERMS Compressive sensing, sparsity averaging, basis pursuit, color eye image.

I. INTRODUCTION

Recently, the medical surgery preparation and disease diagnosis exploit color medical images, which demand the massive size of color medical images and require a lot of space to store the images. For example, a wireless capsule endoscopy (WCE) image with a dimension of 256×256 pixels using 16-bit results in an average of 75 MB for a total of 200-400 images. In addition, eye image analysis can be an alternative for the diagnosis of degenerative diseases, i.e., hypertension/sclerosis [1], [2], [3], [4], [5], [6], cerebral disorders [7], [8], [9], diabetic retinopathy [10], [11], [12], [13], a retinal prosthesis [14], [15], [16], [17], and non-invasive cholesterol level measurement [18], [19], [20], [21]. The eye images require compression techniques for storage and transmissions. In addition, some eye images have a complex feature with the color format. Thus, high-efficiency image compression that considers color features is urgently required. Furthermore, the color feature of medical images is a complex color feature that affects the quality of medical applications,

The associate editor coordinating the review of this manuscript and approving it for publication was Sabah Mohammed.

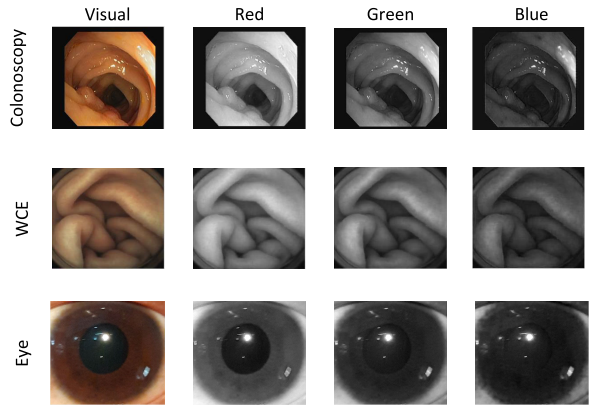

FIGURE 1. A visual of medical images, i.e., Colonoscopy, WCE, and eye image in RGB color space.

then a challenge remains for accurate color medical image compression techniques with good reconstruction quality for medical applications [22].

Two main frameworks were developed for medical image compression (MIC), i.e., lossy and lossless. The example of lossless MIC is advanced video coding or H.264 scheme [23], wavelet-based compression scheme [24], and minimum rate predictors [25]. The example of lossy MIC is interest coding with optimized volume scheme [26], improved video coding [27], adaptive vector quantization with wavelet-based compression framework [28], and hybrid lossy-lossless data compression scheme [29].

Compressive sensing (CS) was proposed to sample a sparse signal using a sampling matrix and a reconstruction method [30], [31], [32]. The CS applications were developed in many fields, such as signal processing [33], wireless communications [34], intelligent transportation systems [35], and watermarking systems [36], [37]. However, CS was approved as an approach that reduces the clinical time in medical imaging [38]. Furthermore, compressed medical imaging (CMI) was proposed as a lossy MIC that exploits CS framework [39].

In addition, a sparsity averaging reweighted analysis (SARA) for radio astronomy image was proposed as a novel sparsity basis prior that average the multiple sparsity basis and exploit BP with RA [40]. Next, a natural image is considered for SARA [41]. The proposed CMI in [39] only considers a single layer or a grayscale format of medical images such as colonoscopy, magnetic resonance imaging, WCE, and computed tomography images. The improvement of M-BRA for CT image was proposed using total variant (TV)-based SARA to improve the visual quality performance and reduce the reconstruction time [42]. For color WCE images, a novel color CMI was proposed using a sparsity averaging (SA) model and reweighted analysis (RA) with three iterations of red green blue (RGB) color space (RGB-SARA) [43]. Next, an initial RGB-based CMI for retinal images using CS reconstruction based on basis pursuit with SA (RGB-BPSA) [44] and total variant (RGB-TV) [45] were proposed. Furthermore, Fig. 1 depicts the example of color medical images such as colonoscopy, WCE, and retinal images in RGB (Red, Green, Blue).

Color feature in the medical image requires good quality for medical diagnosis. Although CS has been extensively investigated, a challenge remains in the processing time of CS reconstruction. Motivated by a reconstruction time reduction of RGB-BPSA, this article proposes an enhancement of RGB-BPSA using a simple SA generated by the combination of Daubechies-1 and Daubechies-8 wavelet filters, called enhanced RGB-BPSA (E-RGB-BPSA). This paper aims for a reduction in reconstruction time while maintaining the color eye image quality. The following are the research contributions of this paper.

- Investigating the effect of SA basis number in RGB-BPSA for CMI of the color eye image.
- Proposing a simple average basis yet efficient to reduce the reconstruction time.
- Proposing variable density sampling (VDS) for CS measurement in E-RGB-BPSA.
- Evaluating the performance of the proposed E-RGB-BPSA on private color eye image datasets.

The rest organization of this paper is presented as follows. In Section II, the related methods are presented to elaborate the CS methods of medical images further specific to color eye images. In Section III, an overview of CMI is presented. In Section IV, the methodology is presented to explain the E-RGB-BPSA in terms of measurement using VDS, simple SA, and reconstruction. In Section V, experiments are presented to explain datasets, performance metrics, experiment setup, and experiment results. In Section VI, the conclusion of this paper is presented.

II. RELATED METHODS

Donoho designed a compressed data acquisition (a signal or digital image) approach which does not require prior knowledge of the signal/image, referred to as compressed sensing [30]. In specific applications, CS reduced sampling time, sampling rate, and the use of analog-to-digital converter resources. In the past decades, CS was studied for theoretical research and technical application of medical imaging [32].

In medical imaging, Sloun et al. [46] propose CS of multiple bases with reweighted analysis [47]. Hashemi et al. propose an approach to reduce the computing of the CS method for computed tomography (CT) images using an active pseudo-polar Fourier and Radon transform. Furthermore, sparse sampling schemes were exploited for CS reconstruction of CT image [48], [49], [50], [51]. Similarly, in magnetic resonance imaging (MRI), CS was investigated as a promising scheme to speedup the MRI acquisition process [52], [53], [54], [55]. Recently, DL-based CS using generative adversarial networks [56], [57], vanilla convolutional neural networks [58], and ADMM-NET [59] were validated to improved reconstruction performance of MRI.

Carrillo et al. [41] proposed the use of multiple dictionaries of wavelet basis using eight Daubechies taps and averaging basis for CS of images such as natural and MRI of brain

images, referred to as SARA. Rahim et al. [39] proposed the improvement of SARA for medical images, i.e, MRI, CT, colonoscopy, and WCE images. In [39], a novel sparsity basis was proposed which was generated from multiple bases of SARA, referred to as multiple basis pursuit with reweighted analysis (M-BRA). The improvement of M-BRA for CT image was proposed by Rahim et al. [42] using TV-based SARA to improve the visual quality performance and reducing the reconstruction time, referred to as TV-SARA. The limitations of the M-BRA and TV-SARA are the resolution of the medical image (64 × 64 pixels) and only grayscale color space. Considers RGB color space, Magdalena et al. [43] proposed a novel CS of RGB-based color medical images using SARA for WCE images, referred to as RGB-SARA. The performance of RGB-SARA was investigated using 256 × 256 pixels and the reconstruction time is high due to reweighted analysis (RA) iterations. SARA consists of two processes, i.e., basis pursuit based on sparsity averaging (BPSA) as the first reconstruction and RA as the second reconstruction. To solve this problem, Rahim et al. [44] proposed RGB-SARA without RA for color eye images, referred to as RGB-BPSA. In addition, Novamizanti et al. [45] proposed TV-based CS for RGB-based color eye images, referred to as RGB-TV.

Previous works have been proposed using spread spectrum Fourier sampling (SSFS) for the measurement of the CS [39], [40], [41], [42], [43], [44], [45]. SSFS is one of the uniform random matrices for sensing matrix in CS. However, this paper proposes a novel VDS for RGB-BPSA to improve the performance of the reconstruction images. Furthermore, Table 1 shows the summary of the related methods.

III. OVERVIEW OF CMI

Throughout this paper, a CS framework based on RGB color space is proposed. Suppose $\boldsymbol{x}$, $\boldsymbol{y}$, and $\hat{\boldsymbol{x}}$ represent a sparse, measured, and reconstructed signal in CS, respectively. Each RGB layer of color medical image is reshaped to $\boldsymbol{x}$ as shown in Fig. 2. The CS consists of measurement and CS reconstruction. This section presents the overview of CMI.

A. CS MEASUREMENT

The aim of this process is to obtain a compressed signal $\boldsymbol{y}$ from a signal $\boldsymbol{x}$ using a sensing matrix $\boldsymbol{\Phi}$ which is determined as

$$\boldsymbol{y} = \boldsymbol{\Phi}\boldsymbol{x}. \tag{1}$$

The matrix multiplication in Eq. (1) requires dimension of $\boldsymbol{x} \in \mathbb{C}^{n\times 1}$, $\boldsymbol{\Phi}$ is $\mathbb{C}^{m\times n}$ with $m \ll n$, and $\boldsymbol{y} \in \mathbb{C}^{m\times 1}$. Clearly, $\boldsymbol{y}$ is represented by less m-number of samples.

Consider a two-dimensional medical image I, then one-dimensional signal $\boldsymbol{s} \in \mathbb{R}^{n\times 1}$ is reshaped from I. Next, synthesis sparsity transform $\boldsymbol{\Psi} \in \mathbb{C}^{n\times n}$ is performed as $\boldsymbol{x} = \boldsymbol{\Psi}\boldsymbol{s}$ and Eq. (1) further defined as

$$\boldsymbol{y} = \boldsymbol{\Phi}\boldsymbol{\Psi}\boldsymbol{s}. \tag{2}$$

B. CS RECONSTRUCTION

The aim of this process is to reconstruct the $\hat{\boldsymbol{x}}$ from $\boldsymbol{y}$ using a known matrix $\boldsymbol{\Phi}$ from CS measurement where a convex problem can model the process as

$$\begin{aligned} &\arg\min_{\hat{\boldsymbol{x}}} \left\|\hat{\boldsymbol{x}}\right\|_1 \\ &\text{subject to } \|\boldsymbol{y} - \boldsymbol{\Phi}\hat{\boldsymbol{x}}\|_2 \leq \varepsilon, \end{aligned} \tag{3}$$

where $\|\cdot\|_1$, $\|\cdot\|_2$, and ε represent the ℓ_1 norm, ℓ_2 norm, and ℓ_2 norm upper bound. According to Eq. (2), the convex problem further defined as

$$\begin{aligned} &\arg\min_{\hat{\boldsymbol{s}}} \left\|\hat{\boldsymbol{s}}\right\|_1 \\ &\text{subject to } \|\boldsymbol{y} - \boldsymbol{\Phi}\boldsymbol{\Psi}\hat{\boldsymbol{s}}\|_2 \leq \varepsilon. \end{aligned} \tag{4}$$

IV. METHODOLOGY

This section presents the proposed E-RGB-BPSA as depicted in Fig. 3(a) and (b) for the measurement and reconstruction, respectively. In measurement, an $N \times N \times 3$ pixels of the color medical image with RGB format (denoted by $\boldsymbol{I} \in \mathbb{Z}^{N\times N\times 3}$) is considered as input medical image. Next, RGB layers are obtained from $\boldsymbol{I}$, and RGB loops are performed to obtain compressed signal $\boldsymbol{y}$. The RGB loops in the compression step are finished when all RGB layers have been processed. While in reconstruction, the compressed signal with noise $\boldsymbol{y}$ is recovered to get $\hat{\boldsymbol{x}}$.

A. PREPARATION

Before the measurement step, a preparation step is performed such as normalize step and enforce positivity step. Fig. 4 shows the example of the preparation steps.

B. MEASUREMENT WITH VARIABLE DENSITY SAMPLING

In this framework of CS [30], [31], the signal is assumed to be compressible or sparse on some basis. The sparse signal $\boldsymbol{x} = \boldsymbol{\Psi}\boldsymbol{s}$ with $\boldsymbol{\Psi} \in \mathbb{R}^{n\times n}$ as the sparsity basis is also considered and it contains only k non-zero values. With an assumption of $k \ll n$, the signal is sufficiently approximated by the first k values. The signal is represented by m linear samples and denoted by a compressed signal $\boldsymbol{y} \in \mathbb{C}^m$ in some sensing matrix $\boldsymbol{\Phi} \in \mathbb{C}^{m\times n}$ and affected by noise $n \in \mathbb{C}^m$. The measurement is defined as

$$\boldsymbol{y} = \boldsymbol{\Theta}\boldsymbol{s} + n, \tag{5}$$

where $\boldsymbol{\Theta} = \boldsymbol{\Phi}\boldsymbol{\Psi} \in \mathbb{C}^{m\times n}$ represents the sensing basis.

Assuming a $N \times N \times 3$ pixels of a color eye image in RGB format (denoted by $\boldsymbol{I} \in \mathbb{R}^{N\times N\times 3}$), the RGB loops are performed to each layer of RGB channel. The RGB loops in the measurement step will be finished when all RGB color layers have been processed. Each loop starts with a preparation process to obtain image $\boldsymbol{P} \in \mathbb{R}^{N\times N}$. After that, the VDS is performed. A signal $\boldsymbol{x} \in \mathbb{R}^{n\times 1}$ is measured by sensing matrix as

$$\boldsymbol{y} = \boldsymbol{\Phi}\boldsymbol{x}, \tag{6}$$

TABLE 1. The summary of related methods.

Method Name	Ref.	Methodology							Resolutions (pixels)	Medical Image				
		SSFS	VDS	SA	BP	TV	RA	RGB		MRI	CT	Colonoscopy	WCE	Eye
SARA	[41]	✓		✓	✓		✓		64×64	✓				
M-BRA	[39]	✓		✓	✓		✓		64×64	✓	✓	✓	✓	
TV-SARA	[42]	✓		✓	✓		✓		64×64		✓			
RGB-SARA	[43]	✓		✓	✓		✓	✓	256×256				✓	
RGB-BPSA	[44]	✓		✓	✓			✓	256×256					✓
RGB-TV	[45]	✓				✓		✓	256×256					✓
This paper			✓	✓	✓			✓	512×512					✓

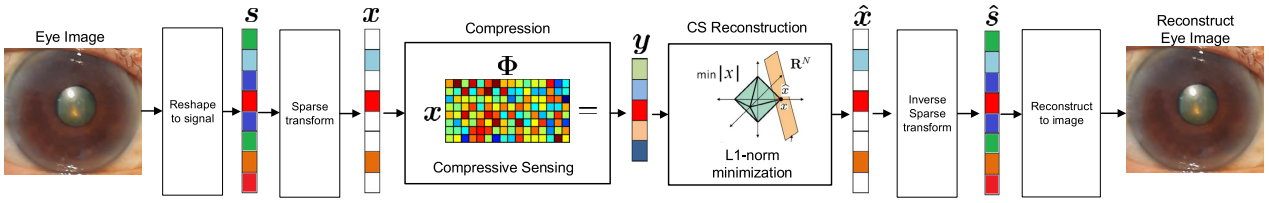

FIGURE 2. The step of CMI for eye image.

where $\mathbf{\Phi}$ represents the measurement matrix with dimension $\mathbb{C}^{m\times n}$. Furthermore, the VDS matrix is determined as

$$\mathbf{\Phi} = \mathbf{MFS}, \tag{7}$$

where $\mathbf{M}$ indicates the mask image, $\mathbf{F}$ represents the discrete Fourier transform coefficients, and $\mathbf{S}$ is the VDS matrix. $\mathbf{M}$, $\mathbf{F}$, and $\mathbf{S}$ are modelled by a rectangular binary matrix $\mathbb{R}^{m\times n}$, complex matrix $\mathbb{C}^{n\times n}$, and a diagonal matrix $\mathbb{R}^{n\times n}$, respectively. In addition, the inverse transform of $\mathbf{MFS}$ is described as

$$\mathbf{F}^{\mathrm{T}}\mathbf{M}^{\mathrm{T}}\mathbf{1}_M, \tag{8}$$

where a binary mask with the matrix of one $\mathbf{1}_M \in \mathbb{R}^M$ is taken into account. Last, when the RGB loops were finished, then $\boldsymbol{y}$ is obtained.

Previous works have been proposed using spread spectrum Fourier sampling (SSFS) for the measurement of the CS [39], [41], [42], [43], [44], [45]. SSFS is one of the uniform random matrices for sensing matrix in CS. Fig. 5 shows the comparison of the SSFS and VDS mask matrix.

C. SIMPLE SA

The sparse signal $\boldsymbol{x}$ can be represented by $\boldsymbol{s} \in \mathbb{C}^D$ with multiple sparsity matrices $\mathbf{\Psi} \in \mathbb{C}^{n\times b}$, where $n < b$ [40]. The SA generates a prior sparse matrix from the average of multiple sparsity matrices [41] and $\mathbf{\Psi}$ becomes

$$\mathbf{\Psi} = \frac{1}{\sqrt{p}} \sum_{i=1}^{p} \mathbf{\Psi}_i, \tag{9}$$

where p represents the number of multiple sparsity matrices. In this paper, similar to RGB-BPSA [44] and RGB-SARA [43], $p = 8$ is considered with Daubechies wavelet filter type and wavelet level decomposition of 4 levels.

In this paper, a simple averaging basis is proposed using a db1-bd8 basis and defined as

$$\mathbf{\Psi} = \frac{1}{\sqrt{2}} \left[\mathbf{\Psi}_1, \mathbf{\Psi}_8\right], \tag{10}$$

D. RECONSTRUCTION

In the reconstruction process, according to the problems in Eq. (5), the ideal approach to recover $\boldsymbol{s}$ is to obtain the sparsest representation $\bar{\boldsymbol{s}}$ recovered from $\boldsymbol{y}$. Thus, a convex problem can model the reconstruction process as

$$\begin{aligned} &\underset{\bar{\boldsymbol{s}}\in\mathbb{C}^n}{\text{minimize}} \ \|\bar{\boldsymbol{s}}\|_0 \\ &\text{subject to } \|y - \Theta\bar{\boldsymbol{s}}\|_2, \end{aligned} \tag{11}$$

where $\|\bar{\boldsymbol{s}}\|_0$ represents the ℓ_0 norm that counts the number of non-zero values in $\bar{\boldsymbol{s}}$. The ℓ_q norm of a complex-valued vector $\boldsymbol{s} \in \mathbb{C}^m$ is defined as $\| \ \|_q = \left(\sum_{i=1}^{M} |\boldsymbol{\alpha}_i|^q\right)^{1/q}$. a convex problem is the most common approach to solve the problem in (11) where ℓ_0 norm is replaced by ℓ_1 norm ([30]).

In reconstruction, a process to recover a color eye image from $\boldsymbol{y}$ is carried out by using E-RGB-BPSA. Algorithm 1 presents the steps of E-RGB-BPSA. This article proposes the sparsity basis $\mathbf{\Phi}$ which is generated by the SA. Then, the RGB loops for reconstruction are performed by using BP to get $\mathbf{\Theta}$ for each RGB layer. And lastly, BP step is stopped when β is less than $\varepsilon \in (0, 1)$ or $j = j_{max}$.

Fig. 6 shows the visual reconstruction of the eye image. Furthermore, Fig. 7 shows the visual of E-RGB-BPSA step in RGB color space.

V. EXPERIMENT

In this section, first, medical images such as colonoscopy, WCE, and retinal images are presented. Second, performance metrics are elaborated to investigate the performance of HSV-CMI. Last, the experiment scenario is explained.

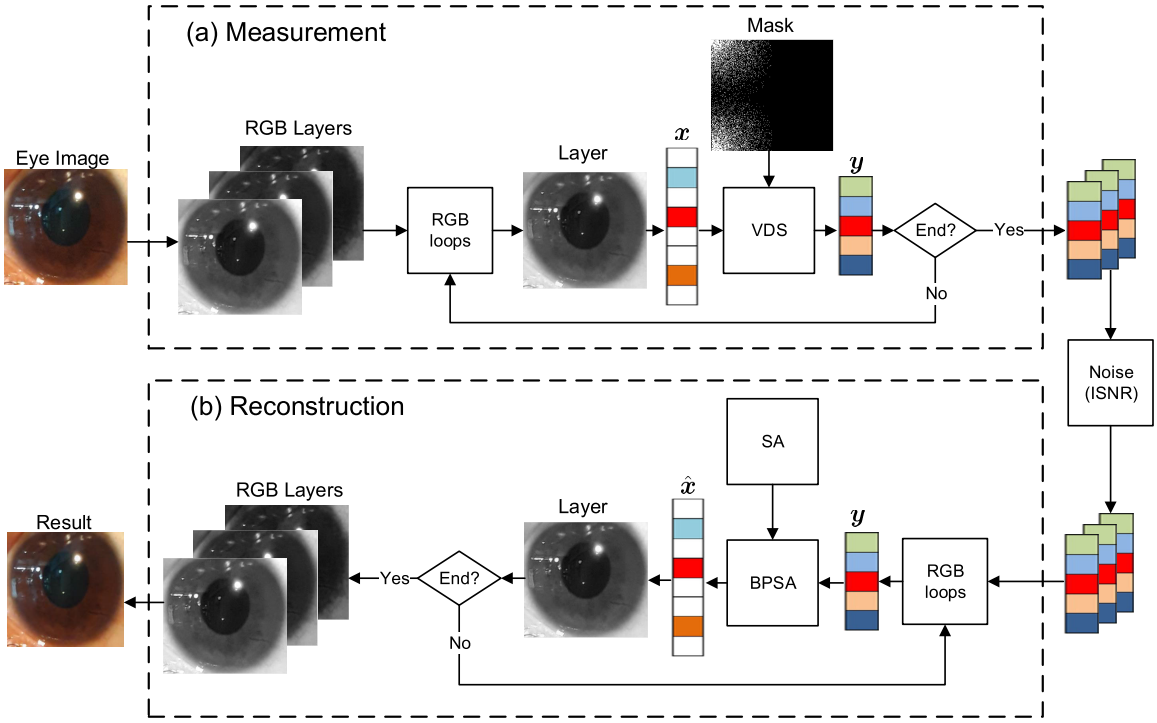

FIGURE 3. Structural details of the E-RGB-BPSA. (a) Measurement using VDS. (b) Reconstruction using E-RGB-BPSA.

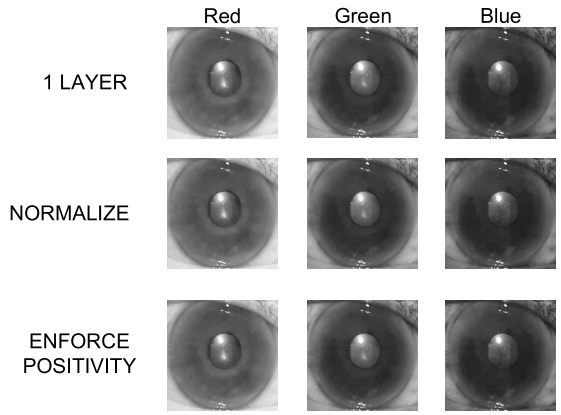

FIGURE 4. A visual of preparation.

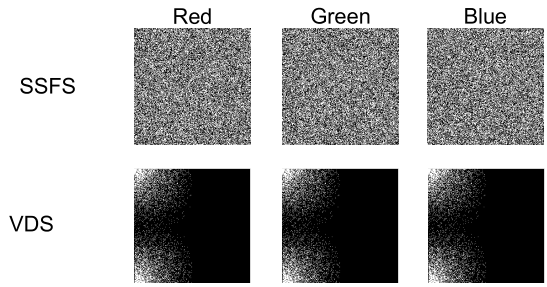

FIGURE 5. A visual of mask matrix of SSFS and VDS.

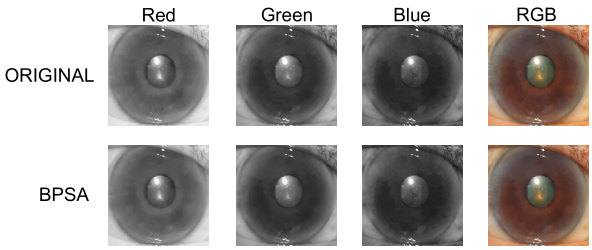

FIGURE 6. A visual of reconstruction step.

A. EYE IMAGES

The color eye images are our private datasets sampled from patients and this study was approved by TelkomMedika hospital, Bandung, Indonesia. The study complied with the guidelines of the Declaration of Helsinki.

Color images were acquired using mobile phone cameras. Images were cropped and normalized to 660 × 603 pixels. There are no public datasets with corresponding eye images for cholesterol measurement, to the best of our knowledge. The private dataset comprises 90 images and split 3 classes of cholesterol levels.

B. PERFORMANCE METRICS

The performance metrics used in this paper are measurement rate (MR), structural similarity (SSIM) index, and signal-to-noise ratio (SNR). The ratio between the size of the measurement image and the image is defined as MR [43] and determined as

$$\mathrm{MR} = \frac{m}{n} \times 100\%, \tag{12}$$

where m and n determine the size of the size of measured signal $\boldsymbol{y}$ and sparse signal $\boldsymbol{x}$.

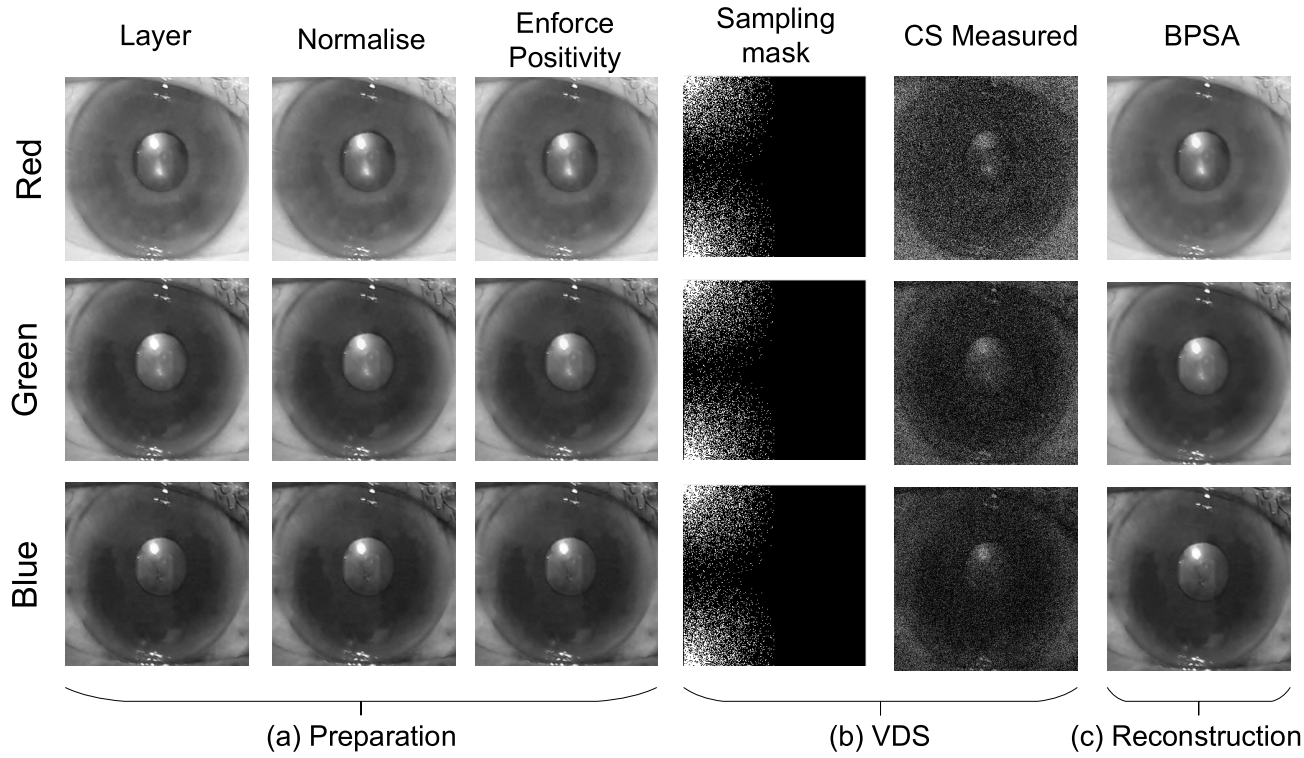

FIGURE 7. A visual of E-RGB-BPSA.

Algorithm 1: E-RGB-BPSA

Input: Compressed signal $\boldsymbol{y} \in \mathbb{C}^m$, sensing basis $\boldsymbol{\Phi} \in \mathbb{C}^{m\times n}$, orthonormal basis $\boldsymbol{\Psi} \in \mathbb{C}^{n\times n}$.
Output: Result image $\hat{\boldsymbol{I}} \in \mathbb{R}^{N\times N\times 3}$.
Generate simple SA basis $\boldsymbol{\Psi} = \frac{1}{\sqrt{2}}[\boldsymbol{\Psi}_1, \boldsymbol{\Psi}_8]$
$i = 1$;
while $i \leq 3$ **do**
  $j = 1$;
  while $j < j_{max}$ *and* $\beta < \varepsilon$ **do**
    $\hat{\boldsymbol{s}}_i^{(j-1)} = \boldsymbol{\Psi}^\dagger \hat{\boldsymbol{x}}_i^{(j-1)}$;
    BP solution
    $\hat{\boldsymbol{x}}_i^{(j)} = \min_{\bar{\boldsymbol{s}}\in\mathbb{C}^m} \left\| \boldsymbol{\Psi}^\dagger \bar{\boldsymbol{s}} \right\|_1$ s.t. $\|\boldsymbol{y} - \boldsymbol{\Phi}\boldsymbol{\Psi}\bar{\boldsymbol{s}}\|_2 \leq \varepsilon$;
    $\beta = \frac{\left\|\hat{\boldsymbol{x}}_i^{(j)} - \hat{\boldsymbol{x}}_i^{(j-1)}\right\|_1}{\left\|\hat{\boldsymbol{x}}_i^{(j-1)}\right\|_1}$;
    $j \leftarrow j + 1$;
  end
  $i \leftarrow i + 1$;
end
Reconstruct $\hat{\boldsymbol{I}}$ from $\hat{\boldsymbol{x}}$;

The SNR [45] is determined as

$$\mathrm{SNR} = \frac{1}{3}\sum_{l=1}^{3} 20\log_{10}\left(\frac{\|\boldsymbol{I}_l\|_2}{\left\|\boldsymbol{I}_l - \hat{\boldsymbol{I}}_l\right\|_2}\right), \tag{13}$$

where l is the RGB color layers of the medical image.

SSIM [44] is an image quality metric between the original color medical image $\boldsymbol{I}$ and the reconstructed color medical image $\hat{\boldsymbol{I}}$. The SSIM is defined as

$$\mathrm{SSIM}(\boldsymbol{I}, \hat{\boldsymbol{I}}) = [l(\boldsymbol{I}, \hat{\boldsymbol{I}})]^\alpha \cdot [c(\boldsymbol{I}, \hat{\boldsymbol{I}})]^\beta \cdot [s(\boldsymbol{I}, \hat{\boldsymbol{I}})]^\gamma, \tag{14}$$

with

$$\begin{aligned} l(\boldsymbol{I}, \hat{\boldsymbol{I}}) &= \frac{2\mu_{\boldsymbol{I}}\mu_{\hat{\boldsymbol{I}}} + \mathrm{A}}{\mu_{\boldsymbol{I}}^2 + \mu_{\hat{\boldsymbol{I}}}^2 + \mathrm{A}}, \\ c(\boldsymbol{I}, \hat{\boldsymbol{I}}) &= \frac{2\sigma_{\boldsymbol{I}}\sigma_{\hat{\boldsymbol{I}}} + \mathrm{B}}{\sigma_{\boldsymbol{I}}^2 + \sigma_{\hat{\boldsymbol{I}}}^2 + \mathrm{B}}, \\ s(\boldsymbol{I}, \hat{\boldsymbol{I}}) &= \frac{\sigma_{\boldsymbol{I}\hat{\boldsymbol{I}}} + \mathrm{C}}{\sigma_{\boldsymbol{I}}\sigma_{\hat{\boldsymbol{I}}} + \mathrm{C}}, \end{aligned} \tag{15}$$

where $l(\boldsymbol{I}, \hat{\boldsymbol{I}})$, $c(\boldsymbol{I}, \hat{\boldsymbol{I}})$, $s(\boldsymbol{I}, \hat{\boldsymbol{I}})$ represent the luminance, contrast, and structure of the image, respectively. μ is the mean of pixels in the image while σ describes the local standard deviation of pixels in the image. $\sigma_{\boldsymbol{I}\hat{\boldsymbol{I}}}$ indicates cross-covariance between $\boldsymbol{I}$. $\hat{\boldsymbol{I}}$, $\mathrm{C} = \frac{\mathrm{B}}{2}$, and $\alpha = \beta = \gamma = 1$ are assumed as default, hence SSIM [44] becomes

$$\mathrm{SSIM}(\boldsymbol{I}, \hat{\boldsymbol{I}}) = \frac{\left(2\mu_{\boldsymbol{I}}\mu_{\hat{\boldsymbol{I}}} + \mathrm{A}\right)\left(2\sigma_{\boldsymbol{I}\hat{\boldsymbol{I}}} + \mathrm{B}\right)}{\left(\mu_{\boldsymbol{I}}^2 + \mu_{\hat{\boldsymbol{I}}}^2 + \mathrm{A}\right)\left(\sigma_{\boldsymbol{I}}^2 + \sigma_{\hat{\boldsymbol{I}}}^2 + \mathrm{B}\right)}. \tag{16}$$

C. EXPERIMENT SCENARIO

The experiment setup to validate the performance of E-RGB-BPSA is simulated using MATLAB R2020b. The specification of the CPU is processor Intel(R) Core(TM)

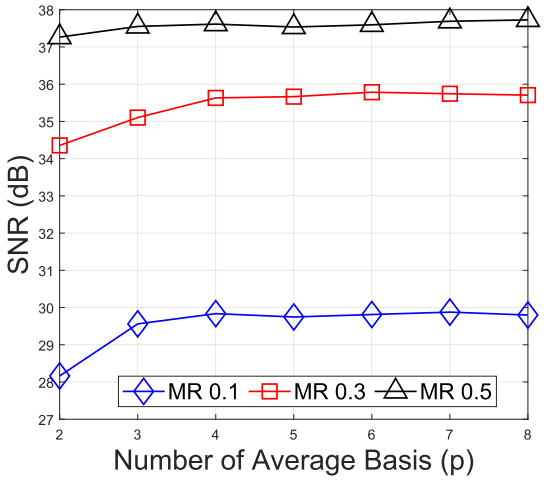

FIGURE 8. The effect of average basis (p) to the SNR results.

TABLE 2. $\mu \pm \sigma$ of SNR results w.r.t p.

Basis (p)	SNR (dB)		
	MR 0.1	MR 0.3	MR 0.5
2	28.16 ± 0.23	34.35 ± 0.32	37.26 ± 0.18
3	29.56 ± 0.10	35.10 ± 0.26	37.55 ± 0.21
4	29.83 ± 0.56	35.63 ± 0.20	37.61 ± 0.27
5	29.74 ± 0.33	35.66 ± 0.34	37.53 ± 0.19
6	29.81 ± 0.42	35.78 ± 0.11	37.59 ± 0.24
7	29.87 ± 0.56	35.74 ± 0.05	37.69 ± 0.11
8	29.79 ± 0.41	35.70 ± 0.18	37.72 ± 0.23

i7-8700 CPU @ 3.20GHz RAM 16GB. Then, the proposed E-RGB-BPSA, RGB-TV [45], and RGB-BPSA [44], are compared. Suppose a 512×512 pixels of medical image is sampled according to MR to get the compressed signal. Next, the reconstruction takes place by using the E-RGB-BPSA, RGB-TV [45], and RGB-BPSA [44], to recover the reconstructed image from the compressed signal and the performance metrics are calculated.

D. SA BASIS SELECTION RESULTS

In SA, the basis Ψ is generated from the wavelet basis with the setting of wavelet filter type, wavelet level (l), and basis number (p). To decide the best p, the performance of RGB-BPSA is presented in terms of SSIM, SNR, and reconstruction time as shown in Figs. 8, 9, and 10, respectively. These figures show the results obtained for the average performance metrics from 90 eye images.

Fig. 8 shows the effect of wavelet basis (p) to the SNR results at MR $= 0.1, 0.3, 0.5$. All MR conditions are saturated at $p = 4$ with results as follows: 28 dB, 34.9 dB, and 37.8 dB at MR $= 0.1, 0.3, 0.5$, respectively.

Fig. 9 shows the effect of wavelet basis (p) to the SSIM results at MR $= 0.1, 0.3, 0.5$. All MR conditions are saturated at $p = 4$ with results as follows: 28 dB, 34.9 dB, and 37.8 dB at MR $= 0.1, 0.3, 0.5$, respectively.

In addition, Fig. 10 presents CPU time with regards to p at MR $= 0.1, 0.3, 0.5$. The increase of p also increases the

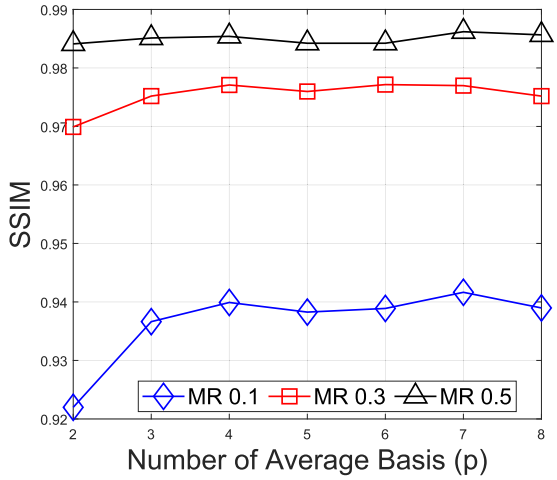

FIGURE 9. The effect of average basis (p) to the SSIM results.

TABLE 3. $\mu \pm \sigma$ of SSIM results w.r.t p.

Basis (p)	SSIM		
	MR 0.1	MR 0.3	MR 0.5
2	0.92 ± 0.003	0.96 ± 0.008	0.98 ± 0.005
3	0.93 ± 0.003	0.97 ± 0.001	0.98 ± 0.008
4	0.93 ± 0.013	0.97 ± 0.009	0.98 ± 0.006
5	0.93 ± 0.009	0.97 ± 0.015	0.98 ± 0.011
6	0.93 ± 0.016	0.97 ± 0.017	0.98 ± 0.012
7	0.94 ± 0.016	0.97 ± 0.018	0.98 ± 0.000
8	0.93 ± 0.011	0.97 ± 0.019	0.98 ± 0.014

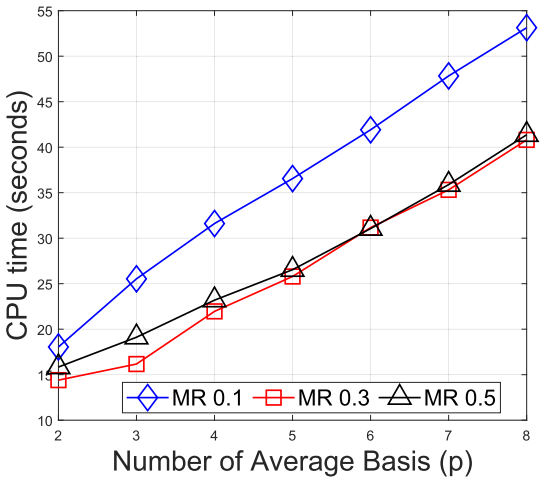

FIGURE 10. The effect of average basis (p) to the BP time results.

CPU time. The longest CPU time is MR $= 0.1$. CMI without sparsity averaging ($p = 1$) is longer than $p = 2$. In [44], $p = 8$ is performed for RGB-BPSA and the results showed that the CPU time achieves 52 seconds. As can be seen in Fig. 10, this paper improves RGB-BPSA with simpler $p = 2$ for sparsity averaging basis and using the combination of db1-db8 rather than db1-db2 for conventional BPSA.

E. LEVEL OF WAVELET BASIS

The level of wavelet basis (l) is investigated, where E-RGB-BPSA and RGB-BPSA are compared in terms of SNR, SSIM, and CPU time with $l = 1, 2, 3, 4$.

TABLE 4. $\mu \pm \sigma$ of CPU time results w.r.t p.

Basis (p)	CPU Time (seconds)		
	MR 0.1	MR 0.3	MR 0.5
2	18.04 ± 0.24	14.40 ± 0.21	15.83 ± 0.10
3	25.53 ± 0.23	16.17 ± 0.80	19.11 ± 0.33
4	31.60 ± 0.74	21.95 ± 0.50	23.18 ± 1.13
5	36.54 ± 0.26	25.79 ± 0.81	26.53 ± 0.96
6	41.91 ± 0.63	31.16 ± 0.62	31.05 ± 0.84
7	47.83 ± 1.39	35.31 ± 0.56	35.88 ± 0.81
8	53.12 ± 1.20	40.80 ± 0.40	41.36 ± 1.29

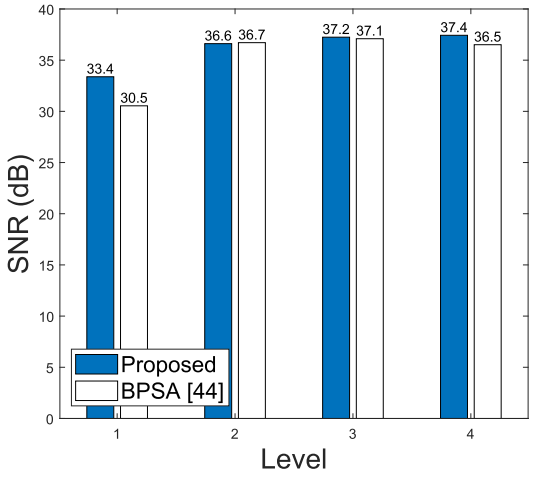

FIGURE 11. The effect of wavelet level (l) to the SNR results.

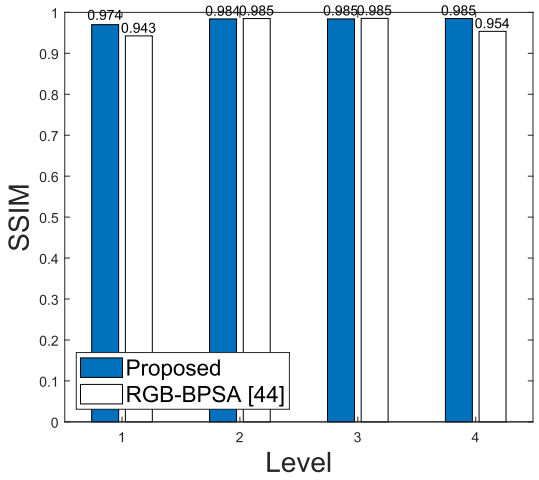

FIGURE 12. The effect of wavelet level (l) to the SSIM results.

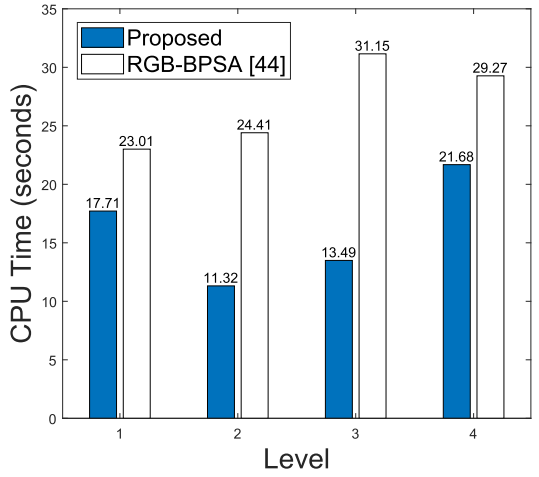

FIGURE 13. The effect of wavelet level (l) to the BP time results.

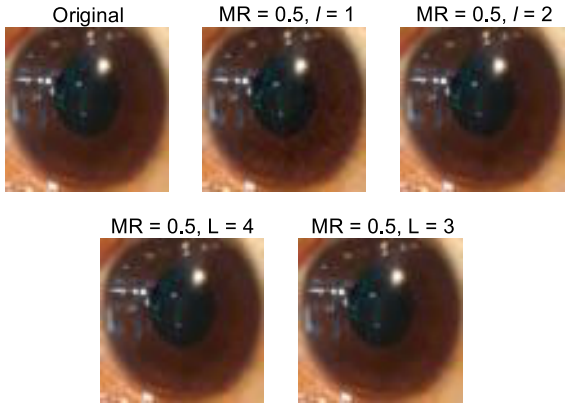

FIGURE 14. A visual of eye image with different l settings in RGB.

First, Fig. 11 presents SNR with regards to l at MR $= 0.5$. The E-RGB-BPSA outperforms the conventional BPSA at $l = 1, 3, 4$ conditions with improvements as follows: 3.1 dB at $l = 1$, 0.1 dB at $l = 3$, and 0.9 dB at $l = 4$. For $l = 2$, the conventional RGB-BPSA outperforms the E-RGB-BPSA with 0.1 dB but the best l result is $l = 4$ with SNR $= 37.4$ dB at MR $= 0.5$.

Next, Fig. 12 displays the effect of wavelet level to SSIM results at MR $= 0.5$. The E-RGB-BPSA outperforms the conventional BPSA at $l = 1, 3, 4$ conditions with improvements as follows: 0.031 at $l = 1$, 0.005 at $l = 3$, and 0.04 dB at $l = 4$. For $l = 2$, the conventional RGB-BPSA outperforms the proposed E-RGB-BPSA with 0.001 dB but the best l result is $l = 4$ with SSIM $= 0.985$ at MR $= 0.5$.

Meanwhile, Fig. 13 shows CPU time with regards to l at MR $= 0.3$. The E-RGB-BPSA outperforms the conventional BPSA at all l conditions with improvements as follows: 5 seconds faster at $l = 1$, 10 seconds faster at $l = 2$, 18 seconds faster at $l = 3$, and 7 seconds faster at $l = 4$. Along with these results, the reconstruction time improvement of the proposed CMI is validated with faster CPU time.

Furthermore, Fig 14 shows the visual of the reconstructed eye image for different l at MR$= 0.5$. From Fig 14, the visual is similar in RGB color space then another way to show the trends in the effect of level is required. Fig 15 shows the figure of merit (FOM) using edge detection to show the quality of the reconstructed eye image.

F. MEASUREMENT RATIO

Fig. 16 shows SNR results and the proposed CMI outperforms the RGB-BPSA and RGB-TV at MR ≥ 0.3 but

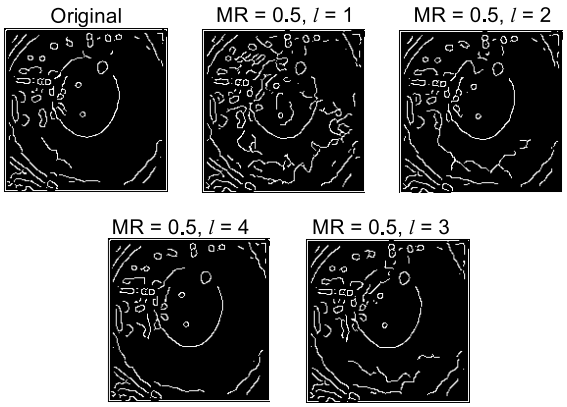

FIGURE 15. A visual of eye image with different *l* settings in FOM.

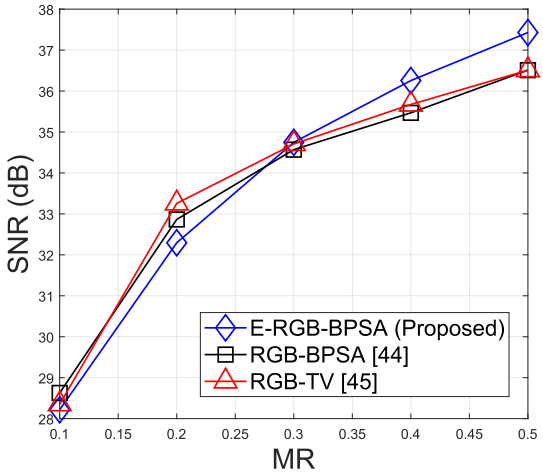

FIGURE 16. SNR results for different MR settings.

shows the worst performance at MR $\leq$ 0.2. The proposed CMI achieves SNR $=$ 38.5 dB at MR $=$ 0.5. For SSIM results, the proposed CMI with E-RGB-BPSA outperforms both RGB-BPSA and RGB-TV with SSIM $\geq$ 0.92 at MR $\geq$ 0.1. Let SSIM $>$ 0.95, it is achieved by the proposed CMI at MR $>$ 0.2 while RGB-BPSA and RGB-TV cannot achieve MR $\leq$ 0.5. Fig. 18 shows reconstruction time with regards to MR $=$ 0.1, 0.2, 0.3, 0.4, 0.5 to investigate E-RGB-BPSA, RGB-BPSA [44], and RGB-TV [45]. CPU time of the proposed CMI is 10 and 40 seconds faster than RGB-BP-SA and RGB-TV, respectively. The effect of MR results validates that the SNR, SSIM, and CPU time of E-RGB-BPSA with resolution 512 $\times$ 512 outperforms the existing RGB-BPSA and RGB-TV.

G. ROBUSTNESS TO THE EFFECT OF INPUT SNR

In this paper, as in Eq. (5), n is a complex Gaussian noise according to an input SNR (ISNR). The ISNR is calculated as

$$\text{ISNR} = 20\log_{10}\left(\frac{\|\Theta s\|_2}{\|n\|_2}\right), \tag{17}$$

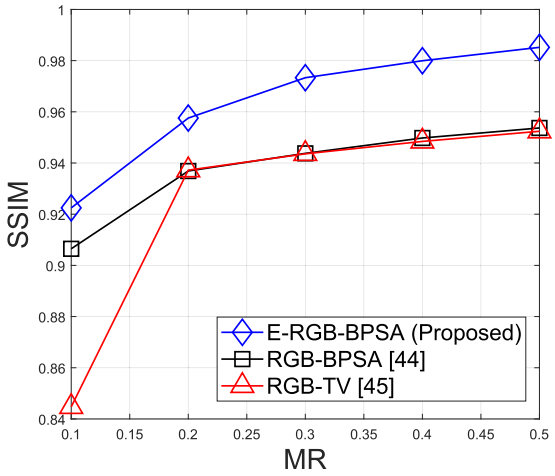

FIGURE 17. SSIM results for different MR settings.

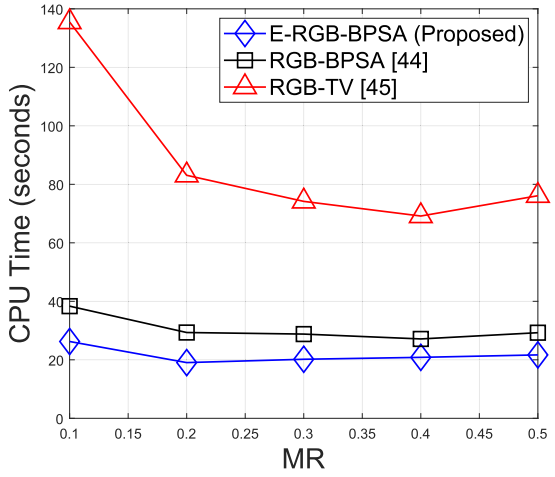

FIGURE 18. BP time results for different MR settings.

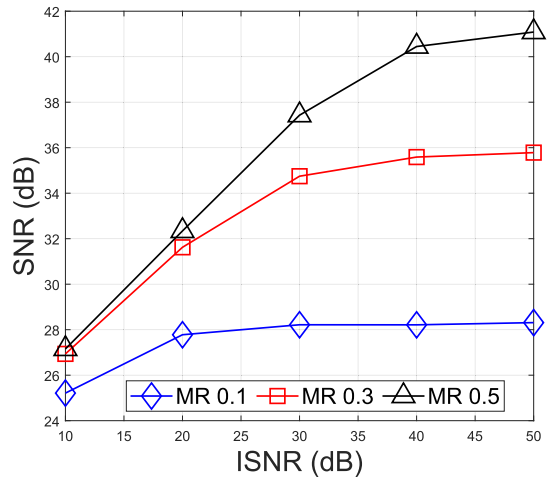

FIGURE 19. SNR results for different ISNR settings.

where Θs is the clean measured signal. To investigate the robustness of E-RGB-BPSA, the effect of ISNR on SNR,

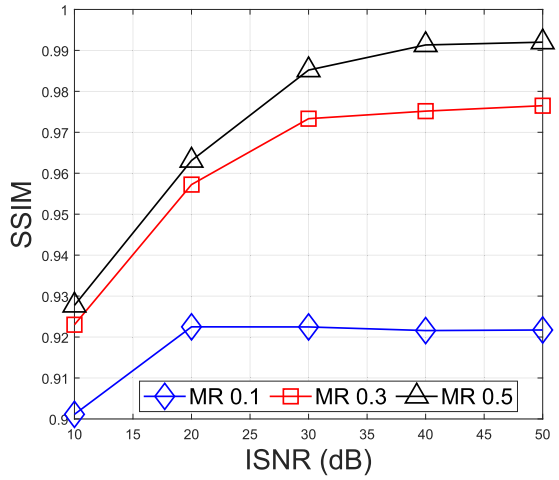

FIGURE 20. SSIM results for different ISNR settings.

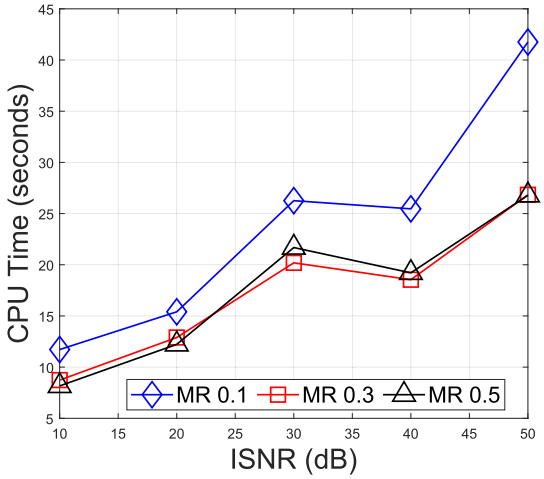

FIGURE 21. BP time results for different ISNR settings.

SSIM, and CPU time is presented. Figs. 19, 20, and 21 show SNR, SSIM, and CPU time results for the robustness to the effect ISNR. MR 0.1, 0.3, 0.5 are investigated and the results show that and the SNR and SSIM shift from high to low as the MR number decreases, while the CPU time shift from high to low as the MR number increases. For MR$=$ 0.1, SNR of 28 dB and SSIM of 0.92 are achieved at ISNR $>$ 20 dB. The CPU time is increased as the ISNR increases.

VI. CONCLUSION

This paper proposes a faster compressed medical imaging (CMI) of color eye images using RGB-BPSA, referred to as E-RGB-BPSA. A simple sparsity averaging basis is proposed using two wavelet basis such as Db1 and Db8 sparsity basis. The SNR, SSIM, and reconstruction time of E-RGB-BPSA outperform the conventional RGB-BPSA for basis pursuit reconstruction. The proposed E-RGB-BPSA with a resolution 512 $\times$ 512 pixels can be compressed into MR $\geq$ 0.1 in SNR $>$ 28 dB and SSIM $>$ 0.92. The reconstruction time of the proposed method is 5 seconds faster than the conventional RGB-BPSA in CMI of color eye image with 3 loops of RGB color space.

For future works, the investigation of the effect of CMI in medical image watermarking systems [36], [37], [60], the deep learning model in reconstruction [61], and multi-domain integrative swin transformer networks [62] can be considered for CMI of CRI.

REFERENCES

[1] C. T. Dollery, P. S. Ramalho, and J. W. Paterson, *Retinal Vascular Alterations in Hypertension*. Berlin, Germany: Springer, 1966, pp. 152–169.
[2] I. Goto, K. Kimoto, S. Katsuki, T. Mimatsu, and I. Hiroshi, "Pathological studies on the intracerebral and retinal arteries in cerebrovascular and non-cerebrovascular diseases," *Stroke*, vol. 6, no. 3, pp. 263–269, May 1975.
[3] M. O. M. Tso and L. M. Jampol, "Pathophysiology of hypertensive retinopathy," *Ophthalmology*, vol. 89, no. 10, pp. 1132–1145, Oct. 1982.
[4] M. O. Tso, G. W. Abrams, and L. M. Jampol, "Hypertensive retinopathy, choroidopathy, and optic neuropathy: A clinical and pathophysiological approach to classification," in *Retinal and Choroidal Manifestations of Selected Systemic Diseases*. Baltimore, MD, USA: Williams & Wilkins, 1991, pp. 79–127.
[5] T. Y. Wong, R. Klein, B. E. K. Klein, J. M. Tielsch, L. Hubbard, and F. J. Nieto, "Retinal microvascular abnormalities and their relationship with hypertension, cardiovascular disease, and mortality," *Surv. Ophthalmol.*, vol. 46, no. 1, pp. 59–80, Jul. 2001.
[6] L. D. Hubbard, R. J. Brothers, W. N. King, L. X. Clegg, R. Klein, L. S. Cooper, A. Sharrett, M. D. Davis, and J. Cai, "Methods for evaluation of retinal microvascular abnormalities associated with hypertension/sclerosis in the atherosclerosis risk in communities study," *Ophthalmology*, vol. 106, no. 12, pp. 2269–2280, Dec. 1999.
[7] M. K. Ikram, F. J. de Jong, J. R. Vingerling, J. C. M. Witteman, A. Hofman, M. M. B. Breteler, and P. T. V. M. de Jong, "Are retinal arteriolar or venular diameters associated with markers for cardiovascular disorders? The Rotterdam study," *Invest. Ophthalmol. Vis. Sci.*, vol. 45, no. 7, pp. 2129–2134, Jul. 2004.
[8] M. K. Ikram, F. J. De Jong, E. J. Van Dijk, N. D. Prins, A. Hofman, M. M. B. Breteler, and P. T. V. M. de Jong, "Retinal vessel diameters and cerebral small vessel disease: The Rotterdam scan study," *Brain*, vol. 129, no. 1, pp. 182–188, Jan. 2006.
[9] V. Joshi, J. Wigdahl, S. Nemeth, C. Manda, S. Lewallen, T. Taylor, I. MacCormick, S. Harding, and P. Soliz, "Automated detection of malarial retinopathy in retinal fundus images obtained in clinical settings," in *Proc. 40th Annu. Int. Conf. IEEE Eng. Med. Biol. Soc. (EMBC)*, Jul. 2018, pp. 5950–5953.
[10] J. Cunha-Vaz, "Pathophysiology of diabetic retinopathy," *Brit. J. Ophthalmol.*, vol. 62, no. 6, pp. 351–355, 1978.
[11] X. Zhang, J. B. Saaddine, C.-F. Chou, M. F. Cotch, Y. J. Cheng, L. S. Geiss, E. W. Gregg, A. L. Albright, B. E. K. Klein, and R. Klein, "Prevalence of diabetic retinopathy in the United States, 2005–2008," *J. Amer. Med. Assoc.*, vol. 304, no. 6, pp. 649–656, Aug. 2010.
[12] A. W. Stitt, T. M. Curtis, M. Chen, R. J. Medina, G. J. McKay, A. Jenkins, T. A. Gardiner, T. J. Lyons, H.-P. Hammes, R. Simó, and N. Lois, "The progress in understanding and treatment of diabetic retinopathy," *Prog. Retinal Eye Res.*, vol. 51, pp. 156–186, Mar. 2016.
[13] M. Z. Atwany, A. H. Sahyoun, and M. Yaqub, "Deep learning techniques for diabetic retinopathy classification: A survey," *IEEE Access*, vol. 10, pp. 28642–28655, 2022.
[14] J. D. Weiland, W. Liu, and M. S. Humayun, "Retinal prosthesis," *Annu. Rev. Biomed. Eng.*, vol. 7, pp. 361–401, Aug. 2005.
[15] J. D. Weiland and M. S. Humayun, "Retinal prosthesis," *IEEE Trans. Biomed. Eng.*, vol. 61, no. 5, pp. 1412–1424, May 2014.
[16] E. Margalit, M. Maia, J. D. Weiland, R. J. Greenberg, G. Y. Fujii, G. Torres, D. V. Piyathaisere, T. M. O'Hearn, W. Liu, G. Lazzi, G. Dagnelie, D. A. Scribner, E. de Juan Jr., and M. S. Humayun, "Retinal prosthesis for the blind," *Surv. Ophthalmol.*, vol. 47, no. 4, pp. 335–356, Jul./Aug. 2002.
[17] M. S. Humayun, J. D. Weiland, G. Y. Fujii, R. Greenberg, R. Williamson, J. Little, B. Mech, V. Cimmarusti, G. Van Boemel, G. Dagnelie, and E. de Juan Jr., "Visual perception in a blind subject with a chronic microelectronic retinal prosthesis," *Vis. Res.*, vol. 43, no. 24, pp. 2573–2581, 2003.

[18] S. N. Andana, L. Novamizanti, and I. N. Apraz Ramatryana, "Measurement of cholesterol conditions of eye image using fuzzy local binary pattern (FLBP) and linear regression," in *Proc. IEEE Int. Conf. Signals Syst. (ICSigSys)*, Jul. 2019, pp. 79–84.

[19] C. A. Nurbani, L. Novamizanti, I. N. A. N. Ramatryana, and N. P. D. P. Wardana, "Measurement of cholesterol levels through eye based on co-occurrence matrix on Android," in *Proc. IEEE Asia Pacific Conf. Wireless Mobile (APWiMob)*, Nov. 2019, pp. 88–93.

[20] J. Raharjo, L. Novamizanti, and I. N. A. Ramatryana, "Cholesterol level measurement through iris image using gray level co-occurrence matrix and linear regression," *ARPN J. Eng. Appl. Sci.*, vol. 14, no. 21, pp. 3757–3763, 2019.

[21] D. Sari, J. Raharjo, and L. Novamizanti, "Cholesterol level detection through eye image using fractal and decision tree," *IOP Conf. Ser., Mater. Sci. Eng.*, vol. 982, no. 1, Dec. 2020, Art. no. 012010, doi: 10.1088/1757-899x/982/1/012010.

[22] T. W. Cabral, M. Khosravy, F. M. Dias, H. L. M. Monteiro, M. A. A. Lima, L. R. M. Silva, R. Naji, and C. A. Duque, "Compressive sensing in medical signal processing and imaging systems," in *Sensors for Health Monitoring*. Amsterdam, The Netherlands: Elsevier, 2019, pp. 69–92.

[23] V. Sanchez, P. Nasiopoulos, and R. Abugharbieh, "Efficient lossless compression of 4-D medical images based on the advanced video coding scheme," *IEEE Trans. Inf. Technol. Biomed.*, vol. 12, no. 4, pp. 442–446, Jul. 2008.

[24] A. Munteanu, J. Cornelis, and P. Cristea, "Wavelet-based lossless compression of coronary angiographic images," *IEEE Trans. Med. Imag.*, vol. 18, no. 3, pp. 272–281, Mar. 1999.

[25] L. F. R. Lucas, N. M. M. Rodrigues, L. A. da Silva Cruz, and S. M. M. de Faria, "Lossless compression of medical images using 3-D predictors," *IEEE Trans. Med. Imag.*, vol. 36, no. 11, pp. 2250–2260, Nov. 2017.

[26] V. Sanchez, R. Abugharbieh, and P. Nasiopoulos, "3-D scalable medical image compression with optimized volume of interest coding," *IEEE Trans. Med. Imag.*, vol. 29, no. 10, pp. 1808–1820, Oct. 2010.

[27] S. Parikh, D. Ruiz, H. Kalva, G. Fernández-Escribano, and V. Adzic, "High bit-depth medical image compression with HEVC," *IEEE J. Biomed. Health Informat.*, vol. 22, no. 2, pp. 552–560, Mar. 2018.

[28] S.-G. Miaou and S.-T. Chen, "Automatic quality control for wavelet-based compression of volumetric medical images using distortion-constrained adaptive vector quantization," *IEEE Trans. Med. Imag.*, vol. 23, no. 11, pp. 1417–1429, Nov. 2004.

[29] D. Rossinelli, G. Fourestey, F. Schmidt, B. Busse, and V. Kurtcuoglu, "High-throughput lossy-to-lossless 3D image compression," *IEEE Trans. Med. Imag.*, vol. 40, no. 2, pp. 607–620, Feb. 2021.

[30] D. L. Donoho, "Compressed sensing," *IEEE Trans. Inf. Theory*, vol. 52, no. 4, pp. 1289–1306, Apr. 2006.

[31] E. J. Candès and M. B. Wakin, "An introduction to compressive sampling," *IEEE Signal Process. Mag.*, vol. 25, no. 2, pp. 21–30, Mar. 2008.

[32] L. Wang, L. Li, L. Jin, L. Jing, B. B. Gupta, and L. Xia, "Compressive sensing of medical images with confidentially homomorphic aggregations," *IEEE Internet Things J.*, vol. 6, no. 2, pp. 1402–1409, Apr. 2019.

[33] S. Zhou, Z. Luo, N. Xiu, and G. Y. Li, "Computing one-bit compressive sensing via double-sparsity constrained optimization," *IEEE Trans. Signal Process.*, vol. 70, pp. 1593–1608, 2022.

[34] H. Wang, J. Fang, H. Duan, and H. Li, "Compressive wideband spectrum sensing and signal recovery with unknown multipath channels," *IEEE Trans. Wireless Commun.*, vol. 21, no. 7, pp. 5305–5316, Jul. 2022.

[35] J. Wang, W. Su, C. Luo, J. Chen, H. Song, and J. Li, "CSG: Classifier-aware defense strategy based on compressive sensing and generative networks for visual recognition in autonomous vehicle systems," *IEEE Trans. Intell. Transp. Syst.*, vol. 23, no. 7, pp. 9543–9553, Jul. 2022.

[36] L. R. Shiddik, L. Novamizanti, I. N. A. N. Ramatryana, and H. A. Hanifan, "Compressive sampling for robust video watermarking based on BCH code in SWT-SVD domain," in *Proc. Int. Conf. Sustain. Eng. Creative Comput. (ICSECC)*, Aug. 2019, pp. 223–227.

[37] M. D. Godole, L. Novamizanti, and I. N. A. Ramatryana, "RS code and compressive sampling on video watermarking-based DWT-SVD," in *Proc. 4th Int. Conf. Inf. Technol., Inf. Syst. Electr. Eng. (ICITISEE)*, Nov. 2019, pp. 541–546.

[38] M. Jacob, J. C. Ye, L. Ying, and M. Doneva, "Computational MRI: Compressive sensing and beyond [from the guest editors]," *IEEE Signal Process. Mag.*, vol. 37, no. 1, pp. 21–23, Jan. 2020.

[39] T. Rahim, L. Novamizanti, I. N. A. Ramatryana, and S. Y. Shin, "Compressed medical imaging based on average sparsity model and reweighted analysis of multiple basis pursuit," *Comput. Med. Imag. Graph.*, vol. 90, Jun. 2021, Art. no. 101927.

[40] R. E. Carrillo, J. D. McEwen, and Y. Wiaux, "Sparsity averaging reweighted analysis (SARA): A novel algorithm for radio-interferometric imaging," *Monthly Notices Roy. Astron. Soc.*, vol. 426, no. 2, pp. 1223–1234, 2012.

[41] R. E. Carrillo, J. D. McEwen, D. Van De Ville, J.-P. Thiran, and Y. Wiaux, "Sparsity averaging for compressive imaging," *IEEE Signal Process. Lett.*, vol. 20, no. 6, pp. 591–594, Jun. 2013.

[42] T. Rahim, L. Novamizanti, I. N. A. Ramatryana, S. Y. Shin, and D. S. Kim, "Total variant based average sparsity model with reweighted analysis for compressive sensing of computed tomography," *IEEE Access*, vol. 9, pp. 119158–119170, 2021.

[43] R. Magdalena, T. Rahim, I. P. A. E. Pratama, L. Novamizanti, I. N. A. Ramatryana, A. Y. Raja, and S. Y. Shin, "RGB-based compressed medical imaging using sparsity averaging reweighted analysis for wireless capsule endoscopy images," *IEEE Access*, vol. 9, pp. 147091–147101, 2021.

[44] T. Rahim, R. Magdalena, I. P. A. E. Pratama, L. Novamizanti, I. N. A. Ramatryana, S. Y. Shin, and D. S. Kim, "Basis pursuit with sparsity averaging for compressive sampling of iris images," *IEEE Access*, vol. 10, pp. 13728–13737, 2022.

[45] L. Novamizanti, I. N. A. Ramatryana, R. Magdalena, I. P. A. E. Pratama, T. Rahim, and S. Y. Shin, "Compressive sampling of color retinal image using spread spectrum Fourier sampling and total variant," *IEEE Access*, vol. 10, pp. 42198–42207, 2022.

[46] S. Hashemi, S. Beheshti, P. R. Gill, N. S. Paul, and R. S. C. Cobbold, "Accelerated compressed sensing based CT image reconstruction," *Comput. Math. Methods Med.*, vol. 2015, pp. 1–16, May 2015.

[47] R. van Sloun, A. Pandharipande, M. Mischi, and L. Demi, "Compressed sensing for ultrasound computed tomography," *IEEE Trans. Biomed. Eng.*, vol. 62, no. 6, pp. 1660–1664, Jun. 2015.

[48] Z. Zhu, K. Wahid, P. Babyn, D. Cooper, I. Pratt, and Y. Carter, "Improved compressed sensing-based algorithm for sparse-view CT image reconstruction," *Comput. Math. Methods Med.*, vol. 2013, pp. 1–15, Mar. 2013.

[49] S. Hua, M. Ding, and M. Yuchi, "Sparse-view ultrasound diffraction tomography using compressed sensing with nonuniform FFT," *Comput. Math. Methods Med.*, vol. 2014, pp. 1–13, Apr. 2014.

[50] G.-H. Chen, J. Tang, and S. Leng, "Prior image constrained compressed sensing (PICCS): A method to accurately reconstruct dynamic CT images from highly undersampled projection data sets," *Med. Phys.*, vol. 35, no. 2, pp. 660–663, 2008.

[51] X. Li and S. Luo, "A compressed sensing-based iterative algorithm for CT reconstruction and its possible application to phase contrast imaging," *Biomed. Eng. OnLine*, vol. 10, no. 1, p. 73, 2011.

[52] J. Huang, S. Zhang, and D. Metaxas, "Efficient MR image reconstruction for compressed MR imaging," *Med. Image Anal.*, vol. 15, no. 5, pp. 670–679, Oct. 2011.

[53] Y. Liu, Z. Zhan, J.-F. Cai, D. Guo, Z. Chen, and X. Qu, "Projected iterative soft-thresholding algorithm for tight frames in compressed sensing magnetic resonance imaging," *IEEE Trans. Med. Imag.*, vol. 35, no. 9, pp. 2130–2140, Sep. 2016.

[54] B. Zhao, J. P. Haldar, A. G. Christodoulou, and Z.-P. Liang, "Image reconstruction from highly undersampled (k,*t*)-space data with joint partial separability and sparsity constraints," *IEEE Trans. Med. Imag.*, vol. 31, no. 9, pp. 1809–1820, Sep. 2012.

[55] Q. Liu, S. Wang, K. Yang, J. Luo, Y. Zhu, and D. Liang, "Highly undersampled magnetic resonance image reconstruction using two-level Bregman method with dictionary updating," *IEEE Trans. Med. Imag.*, vol. 32, no. 7, pp. 1290–1301, Jul. 2013.

[56] T. M. Quan, T. Nguyen-Duc, and W.-K. Jeong, "Compressed sensing MRI reconstruction using a generative adversarial network with a cyclic loss," *IEEE Trans. Med. Imag.*, vol. 37, no. 6, pp. 1488–1497, Jun. 2018.

[57] M. Mardani, E. Gong, J. Y. Cheng, S. S. Vasanawala, G. Zaharchuk, L. Xing, and J. M. Pauly, "Deep generative adversarial neural networks for compressive sensing MRI," *IEEE Trans. Med. Imag.*, vol. 38, no. 1, pp. 167–179, Jan. 2019.

[58] S. Wang, Z. Su, L. Ying, X. Peng, S. Zhu, F. Liang, D. Feng, and D. Liang, "Accelerating magnetic resonance imaging via deep learning," in *Proc. IEEE 13th Int. Symp. Biomed. Imag. (ISBI)*, Apr. 2016, pp. 514–517.

[59] J. Sun, Y. Yang, H. Li, and Z. Xu, "Deep ADMM-net for compressive sensing MRI," in *Proc. Adv. Neural Inf. Process. Syst.*, vol. 29, 2016, pp. 1–9.
[60] N. S. Utami, L. Novamizanti, S. Saidah, and I. N. A. Ramatryana, "SVD on a robust medical image watermarking based on SURF and DCT," in *Proc. IEEE Int. Conf. Ind. 4.0, Artif. Intell., Commun. Technol. (IAICT)*, Jul. 2021, pp. 32–38.
[61] W. Wu, D. Hu, W. Cong, H. Shan, S. Wang, C. Niu, P. Yan, H. Yu, V. Vardhanabhuti, and G. Wang, "Stabilizing deep tomographic reconstruction," 2020, *arXiv:2008.01846*.
[62] J. Pan, H. Zhang, W. Wu, Z. Gao, and W. Wu, "Multi-domain integrative swin transformer network for sparse-view tomographic reconstruction," 2021, *arXiv:2111.14831*.

GANDEVA BAYU SATRYA (Senior Member, IEEE) received the Ph.D. degree in security communication for next-generation networks in IT convergence engineering from the School of Electronic Engineering, Kumoh National Institute of Technology, South Korea, in December 2018.

From June 2008 to December 2010, he was a BSS Engineer at PT. ZTE Indonesia, Jakarta, Indonesia. He has been a Lecturer and a Researcher with the School of Applied Science, Telkom University, Bandung, Indonesia, since February 2011. He has been a member of the Research Center of Internet of Things (RC IoT) with Telkom University, since 2019. He is currently appointed as a Technical Activities Coordinator with the IEEE Communication Society (ComSoc) Indonesian Section. His research interests include routing protocol, post-quantum cryptography, security communication in next-generation networks, and applied deep learning.

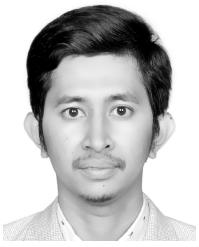

I. NYOMAN APRAZ RAMATRYANA (Member, IEEE) received the bachelor's degree in telecommunication engineering and the master's degree in electrical engineering from Telkom University, Indonesia, in 2010 and 2014, respectively. Currently, he is pursuing the Ph.D. degree in IT convergence engineering with the Kumoh National Institute of Technology, South Korea. His areas of expertise are signal processing, artificial intelligence (AI), wireless communications, and computer vision. His research interests include random access (RA), Raptor coding, non-orthogonal multiple access (NOMA), multiple-input multiple-output (MIMO) antenna, compressed imaging, medical imaging, and deep learning (DL).

LEDYA NOVAMIZANTI (Member, IEEE) received the bachelor's degree in mathematics from Andalas University, in 2005, and the master's degree in electrical and telecommunication engineering from Telkom University, in 2008. Currently, she is pursuing the doctoral degree with the Institut Teknologi Bandung. Since 2010, she has been working as a Lecturer with Telkom University. Her current research interests include image processing, computer vision, data hiding, and machine learning. She received the LPDP Scholarship for her doctoral degree.

SOO YOUNG SHIN (Senior Member, IEEE) received the B.S., M.S., and Ph.D. degrees in electrical engineering and computer science from Seoul National University, South Korea, in 1999, 2001, and 2006, respectively. He was a Visiting Scholar at the FUN Laboratory, University of Washington, USA, from July 2006 to June 2007. He worked at the WiMAX Design Laboratory, Samsung Electronics, for three years. He has been a Professor with the School of Electronics, Kumoh National Institute of Technology, since May 2022. His research interests include wireless LAN, WPAN, WBAN, wireless mesh networks, sensor networks, coexistence among wireless networks, industrial and military networks, cognitive radio networks, and next generation mobile wireless broadband networks.